

Femtosecond Time-Resolved Raman Signals on Ultrafast Dynamics in All-*trans*-β-Carotene

Masayuki Yoshizawa,* Hirokazu Aoki, and Hideki Hashimoto†

Department of Physics, Graduate School of Science, Tohoku University, Aramaki-aza-aoba, Aoba-ku, Sendai 980-8578

†Department of Materials Science and Chemical Engineering, Faculty of Engineering, Shizuoka University, Johoku, Hamamatsu 432-8561

(Received August 29, 2001)

Raman signals of excited states in all-*trans*-β-carotene have been investigated using recently developed femtosecond time-resolved Raman spectroscopy. The Raman signals are distinguished from other absorbance changes due to highly excited states using temporal and spectral dependence on the Raman pump pulse. The negatively stimulated Raman signals due to the $2Ag^-$ excited state are explained by the Raman transition from the vibrational excited levels. The vibrational relaxation of the $2Ag^-$ state has fast and slow kinetics. The fast one has a time constant of 0.6 ps, but the other is slower than the internal conversion to the ground state. Since the molecule exists in the vibrationally excited levels through the relaxation kinetics, the vibrational features in β-carotene are quite important with relation to energy transfer in photosynthesis.

Carotenoids play an important role of light-harvesting in bacterial photosynthesis.[1,2] All-*trans*-β-carotene (β-carotene) is a typical carotenoid with a linear polyene structure (C_{2h} symmetry): it has also attracted much interest in relation to conjugated polymers. Since the ground state of the all-*trans*-carotenoid has A_g^- symmetry, the lowest optically allowed excited state is a $1B_u^+$ state. However, two optically forbidden states, $1B_u^-$ and $2A_g^-$, exist below the $1B_u^+$ state.[3,4] Relaxation kinetics in the carotenoids has been intensively investigated using time-resolved spectroscopy.[5–15] The photogenerated $1B_u^+$ state converts to the $2A_g^-$ state within 100–300 fs. The $1B_u^-$ state has been expected to be an intermediate state during this relaxation pathway.[4,14,15] The $2A_g^-$ state relaxes to the $1A_g^-$ ground state within several picoseconds. The lifetimes of the carotenoids in the light-harvesting complexes become shorter due to ultrafast energy transfer reactions from carotenoids to bacteriochlorophyll.[8,11]

The vibrational relaxation of electronic excited states in large molecules has been considered to be faster than 1 ps generally.[16] Femtosecond fluorescence spectroscopy has determined the vibrational relaxation time of the $1B_u^+$ state in β-carotene to be shorter than 100 fs.[6,10] Femtosecond absorption spectroscopy has found subpicosecond spectral changes due to the vibrational relaxation of the $2A_g^-$ state.[7] Therefore, the energy transfer in the photosynthesis has been assumed to occur from the lowest vibrational level of the excited states.[17] However, Zhang et al. have recently reported that the vibrational relaxation of the $2A_g^-$ state in all-*trans*-lycopene is slower than the internal conversion to the ground state.[9] The vibrational relaxation in carotenoids is very important to understand the energy transfer mechanism in the photosynthesis.

The time-resolved absorption spectroscopy is not suitable to investigate the vibrational relaxation, because it is difficult to assign the 0–0 transition and the vibrational modes. Recent sub-10 fs time-resolved studies can observe transient oscillation due to photoinduced vibrations, but the observed signals are mainly due to the ground state.[13] Time-resolved Raman signals in β-carotene have been observed by picosecond Raman spectroscopy.[12,18,19] The signal due to the C=C stretching vibration (the ν_1 mode) of the $1A_g^-$ ground state at 1521 cm^{-1} decreases due to the photoexcitation, thus the signal due to the same mode of the $2A_g^-$ state appears at 1777 cm^{-1}. The abnormally high frequency in the $2A_g^-$ state has been explained in terms of the vibronic coupling between the $2A_g^-$ and $1A_g^-$ states through the ν_1 mode. However, the temporal dependence of the Raman signal has not been time-resolved.

The time-resolved Raman spectroscopy has been recognized as a powerful method for studying vibrations in photogenerated transient states. The basic technique has been established in the nanosecond region and has been developed to the picosecond region.[20–25] However, the ordinary method cannot have good spectral resolution in the femtosecond region because of the transform limit of a single pulse. The bandwidth of a 100 fs pulse is broader than 100 cm^{-1}. Therefore, only a few femtosecond time-resolved Raman experiments have been reported.[26–29] Recently, we have developed novel femtosecond time-resolved Raman spectroscopy which can measure the Raman signal with femtosecond time resolution and good spectral resolution.[30]

Here, we present the study of the photoexcited states in all-*trans*-β-carotene using the femtosecond time-resolved Raman spectroscopy. The photoinduced absorbance change has also been measured and compared with the Raman signals. Since the excited states undergo transitions to highly excited states, the resonance effect is taken into account during the analysis of the results. The Raman signal is distinguished from other

resonant signals by using spectral features and dependence on the Raman pump pulses. The relaxation kinetics in β-carotene is discussed considering the vibrational relaxation of the excited states.

Experimental

Novel time-resolved Raman spectroscopy measures stimulated Raman scattering of transient states using three optical pulses. Figure 1(a) shows a schematic diagram of measurements using the Raman gain process. A excited state e is initially photogenerated by a pump pulse; it soon converts to a transient state a. The Raman gain signal of the transient state is induced by a Raman pump pulse ω_R and is probed by a supercontinuum pulse ω_S. The time-resolved Raman signal is measured by changing the delay time between the first pump pulse and the other pulses. Temporal resolution of this method is determined by the pump and probe pulses, while spectral resolution is determined by the Raman pump pulse. Therefore, combination of the ultrashort pump and probe pulses and the narrow bandwidth Raman pump pulse can measure the femtosecond Raman signal with good spectral resolution.[30]

The Raman signal observed by the novel method is theoretically calculated as follows. The transient state a generated by the first pump pulse is assumed to have population

$$N(t_d) = \begin{cases} 0 & (t_d < 0) \\ N_0 e^{-t_d/T_N} & (t_d \geq 0) \end{cases} \quad (1)$$

where t_d is a delay time after the pump pulse and T_N is a lifetime of the transient state. The initial and final states of the Raman process are a and c in Fig. 1(a), respectively. Resonance of the Raman pump pulse to a highly excited state b is taken into account. Nonlinear polarizability concerning the Raman gain is obtained as

$$\begin{aligned} P^{(3)}(t) = & -\left(\frac{\mu}{i\hbar}\right)^3 \int_{-\infty}^{t} dt_1 \int_{-\infty}^{t_1} dt_2 \int_{-\infty}^{t_2} dt_3 N(t_3) \\ & \times E_R^*(t_3) e^{i(\omega_R - \omega_{ba})t_3} e^{-(T_{ba}^{-1} + T_N^{-1})(t_2 - t_3)} \\ & \times E_S(t_2) e^{-i(\omega_S - \omega_{bc})t_2} e^{-(T_{ca}^{-1} + T_N^{-1})(t_1 - t_2)} \\ & \times E_R(t_1) e^{-i(\omega_R - \omega_{ba})t_1} e^{-(T_{bc}^{-1} + T_N^{-1})(t - t_1)} e^{-i\omega_{bc}t} \end{aligned} \quad (2)$$

where μ is the dipole moment, $\omega_{\alpha\beta}$ and $T_{\alpha\beta}$ denote, respectively, the transition frequency and the dipole decay time between α and β states, and $E_R(t)e^{-i\omega_R t}$ and $E_S(t)e^{-i\omega_S t}$ are electric fields of the Raman pump and probe pulses, respectively. In this study, we assume that the Raman pump pulse is an exponential pulse:

$$E_R(t) = E_{R0} e^{-\gamma_R |t - t_d + \Delta t|} \quad (3)$$

and the probe pulse is infinitely short:

$$E_S(t) = E_{S0} \delta(t - t_d). \quad (4)$$

Here, γ_R corresponds to the bandwidth of the Raman pump pulse and Δt is the time difference between the probe and the Raman pump pulses.

In the case of off resonance ($\omega_{bc} \to +\infty$), the nonlinear susceptibility for $\Delta t = 0$ is calculated as

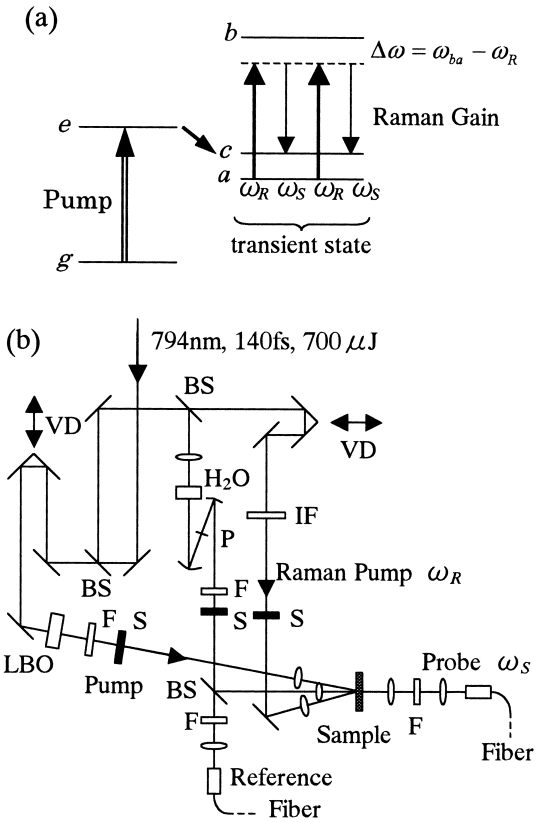

Fig. 1. (a) Schematic diagram of time-resolved Raman spectroscopy (Raman gain). g and e represent the ground state and an initially photoexcited state, respectively. a and c represent the vibrational ground and excited levels in a transient state, respectively. b represents a higher excited state. (b) Experimental setup of femtosecond time-resolved Raman spectroscopy. BS: beam splitters, VD: variable delays, LBO: a LiB_3O_5 crystal, F: filters, S: shutters, IF: an interference filter, H_2O: a water cell, and P: a pin hole.

$$\chi_{OR}^{(3)}(\omega, t_d) \propto \begin{cases} 0 & (t_d < 0) \\ \dfrac{N_0 e^{-t_d/T_n}}{\omega - \omega_{RG} + i(\gamma_v + \gamma_R)} & (t_d \geq 0) \end{cases} \quad (5)$$

where $\omega_{RG} = \omega_R - \omega_{ca}$ and $\gamma_v = T_{ca}^{-1} + T_N^{-1}$ are, respectively, frequency and bandwidth of the Raman line. Since the transmittance change of the probe pulse is determined by the imaginary part of the nonlinear susceptibility, the temporal signal follows the population of the transient state. The extreme temporal resolution is caused by the assumption of the delta-function probe pulse. The spectrum can be observed with the resolution of γ_R independent of the probe pulse.

Figure 1(b) shows the experimental setup. The femtosecond light source was a combination of a mode-locked Ti:sapphire laser (Avesta) and a kHz regenerative amplifier (Spectra Physics, Spitfire). Typical characteristics of the amplified pulse were pulse energy of 700 μJ at 794 nm and duration of 140 fs. The pulse was separated to three beams. The first beam was delayed using an optical variable delay and passed through a 3 mm LBO (LiB_3O_5) crystal. The second harmonic pulse (397 nm) with energy of 35 μJ was used as the first pump pulse. The second beam was fo-

cused into a 10 mm cell containing water. The generated supercontinuum was focused on a pin hole (70 μm) to stabilize the beam profile. The supercontinuum was split to probe and reference pulses. They were focused on respective optical fibers and detected by a spectrometer with a CCD detector (JOBIN YVON, SR460). The last beam was delayed using the other optical variable delay and passed through an interference filter with center wavelength of 794.7 nm and finally used as the Raman pump pulse. The bandwidth and pulse energy of the Raman pump pulse were 23 cm^{-1} and 25 μJ, respectively. The probe and Raman pump pulses were focused on each sample simultaneously (Δt = 0.0 ps). The stimulated Raman signal was obtained as the change induced by the Raman pump pulse. The transmittance change $\Delta T/T$ was calculated and averaged as absorbance change $\Delta A = -\log_{10}(1+\Delta T/T)$ by a personal computer which controlled the variable delays and shutters. The photoinduced absorbance change of the sample was also measured after blocking the Raman pump pulse with a shutter.

The photon densities of the 397 nm pump pulse on the sample were 4×10^{15} and 2×10^{16} photons/cm^2 for the absorption and Raman measurements, respectively. The photon density of the Raman pump pulse was 6×10^{16} photons/cm^2. The durations of the 397 nm pump and Raman pump pulses were 200 fs and 700 fs, respectively. The temporal resolution of the instrument was determined to be 300 fs by the crosscorrelation signal between the 397 nm pump pulse and the probe supercontinuum. The spectral resolution was obtained as 25 cm^{-1} from FWHM of the Raman pump spectrum detected by the spectrometer. Sensitivity of the absorbance change was better than 10^{-3}. The linear polarizations of the pulses were parallel to each other.

All-*trans*-β-carotene was purchased from Wako Pure Chemical Industries Ltd., and recrystallized twice from benzene. Concentrations in the benzene solution for the femtosecond absorption and Raman measurements were 8×10^{-5} M and 4×10^{-4} M, respectively. The solution was circulated using a 1 mm flow cell. The measurements were performed at room temperature.

Results and Discussion

Photoinduced Absorbance Change. The time-resolved absorbance changes of β-carotene after the 397 nm (25190 cm^{-1}) photoexcitation are shown in Fig. 2. The changes have three structures, bleaching at 19500–24000 cm^{-1}, absorption at 16500–19000 cm^{-1}, and absorption around 10000 cm^{-1}. A sharp negative peak at 21980 cm^{-1} is assigned to the Raman gain of C–H stretching modes in β-carotene and benzene, because it is observed when the pump and probe pulses arrive at the sample simultaneously. The temporal responses of the absorbance changes are shown in Fig. 2(b). The solid curves are the best fitted curves considering exponential rise and decay components with convolution of the resolution time. The absorption at 10000 cm^{-1} appears instantaneously after the photoexcitation and disappears with a lifetime of 0.35 ± 0.05 ps. The bleaching at 21500 cm^{-1} appears instantaneously and disappears with a lifetime of 8.8 ± 0.2 ps. The response at 17500 cm^{-1} has three components: a 0.35 ps fast rise, a 8.8 ps decay, and the other slow rise component with a time constant of 1 ps.

Since the absorption around 17500 cm^{-1} is assigned to the transition from the $2A_g^-$ state to a higher excited state, the 0.35 ps time constant corresponds to the formation time of the $2A_g^-$ state. The lifetime of the $2A_g^-$ state is 8.8 ps. The absorption

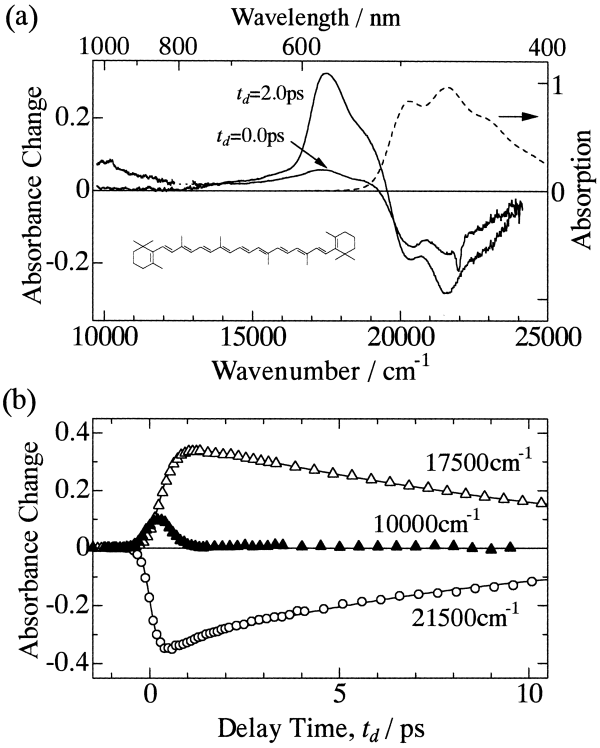

Fig. 2. Time-resolved absorbance changes induced by the 397 nm pump pulse. (a) Absorbance change at delay times of t_d = 0.0 and 2.0 ps. A dashed curve is absorption spectrum without photoexcitation. Inset shows the structure of all-*trans*-β-carotene. (b) Transient absorbance changes at several wavenumbers. Solid curves are the best fits to the data assuming exponential rise and decay components.

around 10000 cm^{-1} cannot be assigned to either the $1B_u^+$ or $1B_u^-$ state, because the relaxation from the initially photoexcited $1B_u^+$ state to the $2A_g^-$ state is expected to pass through the $1B_u^-$ state. The absorption peak at 17500 cm^{-1} becomes sharp with the time constant of 1 ps. Similar spectral changes have been observed in other carotenoids and have been explained by vibrational relaxation of the $2A_g^-$ state.[7,9]

Distinction of Raman Signals. The signals induced by the Raman pump pulse contain the changes due to the resonant excitation, because the photoexcited β-carotene has a weak transient absorption at 794 nm, as shown in Fig. 2(a). Considering the resonance to the highly excited state b, we can calculate the nonlinear susceptibility of the Raman gain signal from Eq. 2 as

$$\chi^{(3)}_{RG}(\omega,t_d) \propto \frac{1-e^{-(T_{ba}^{-1}-i\Delta\omega)t_d}}{\Delta\omega^2+T_{ca}^{-2}}\cdot\frac{N_0e^{-t_d/T_N}}{\omega-\omega_{RG}+i(\gamma_v+\gamma_R)} \quad (6)$$

for $t_d > 0$. Another term with frequency ω_{bc} obtained from Eq. 2 is neglected, because it corresponds to the resonant fluorescence from the state b. The calculated result shows the resonance enhancement, but the initial temporal response is modulated by the decay time T_{ba} and the detuning $\Delta\omega = \omega_{ba}-\omega_R$. In the case of longer delay times ($t_d >> T_{ba}$, $\Delta\omega^{-1}$), the temporal dependence follows the population of the transient state.

Therefore, the time-resolved Raman signal can be measured even in the resonant case.

The stimulated Raman signal on the anti-Stokes side is called Raman loss, because the intensity of the probe pulse is usually decreased by the Raman process. The resonant effect of the Raman loss signal is obtained in a similar way to that used with the Raman gain as

$$\chi^{(3)}_{RL}(\omega,t_d) \propto -\frac{1}{\left(\Delta\omega' + iT_{ca}^{-1}\right)^2}\cdot\frac{N_0 e^{-t_d/T_N}}{\omega-\omega_{RL}+i(\gamma_v+\gamma_R)} \quad (7)$$

where $\Delta\omega' = \omega_{bc}-\omega_R$ is detuning in the Raman loss process and $\omega_{RL} = \omega_R+\omega_{ca}$ is the Raman loss frequency. The resonant fluorescence term with frequency ω_{ba} is neglected. The Raman signal follows the population of the transient state, but the resonant term is complex. Therefore, the spectrum differs from a Lorentzian shape in the case of near resonance. It may be inverse and dispersive.[31]

The resonant signal due to the photoexcitation to highly excited states has a broad spectrum in general, while the Raman line has a sharp peak and shifts following the Raman pump frequency. Therefore, the Raman signal can be distinguished from the spectral feature. Figure 3 shows the absorbance changes induced by the Raman pump pulses with different frequencies. The center frequency of the Raman pump pulse was changed by tilting the interference filter. The delay time after the 397 nm pump pulse was $t_d = 0.7$ ps. The broad absorbance changes due to the highly excited states are subtracted previously. Four positive peaks and a negative peak around 14350 cm^{-1} are found in the signals. Since all the peaks shift following the Raman pump frequency, they are assigned to the stimulated Raman signals. Assignments of the peaks are discussed later.

The Raman signal can be distinguished also by the dependence on the time difference between the probe and the Raman pump pulses Δt. In the case of off resonance, the nonlinear susceptibility of the Raman gain signal for $t_d > 0$ is obtained as

$$\chi^{(3)}_{RG}(\omega,t_d) \propto = \begin{cases} \left[\dfrac{e^{(\gamma_v+\gamma_R)\Delta t}}{\omega-\omega_{RG}+i(\gamma_v+\gamma_R)} + \dfrac{e^{2\gamma_R\Delta t}-e^{(\gamma_v+\gamma_R)\Delta t}}{\omega-\omega_{RG}+i(\gamma_v-\gamma_R)}\right] N_0 e^{-t_d/T_N} & (\Delta t < 0) \\ \dfrac{e^{-(\gamma_v+\gamma_R)\Delta t}}{\omega-\omega_{RG}+i(\gamma_v+\gamma_R)} N_0 e^{-t_d/T_N} & (\Delta t \geq 0) \end{cases} . \quad (8)$$

The temporal dependence on Δt follows roughly the shape of the Raman pump pulse and the signal has a maximum at $\Delta t = 0$. The signal for $\Delta t > 0$ has the bandwidth of $\gamma_v + \gamma_R$. On the other hand, the signal for $\Delta t < 0$ has two terms with bandwidths of $\gamma_v + \gamma_R$ and $\gamma_v - \gamma_R$. Figure 4 shows the Raman signals induced by the Raman pump pulses with different time differences. The signals at $\Delta t = -0.5$ and 0.5 ps are about one fourth of those at $\Delta t = 0.0$ ps. Such values are consistent with the duration of the Raman pump pulse. The lines at $\Delta t = -0.5$ ps have narrower bandwidths. Especially the line at 990 cm^{-1} shows an oscillatory structure. These spectral features can be interpreted by interference of two terms in Eq. 8 for $\Delta t < 0$.

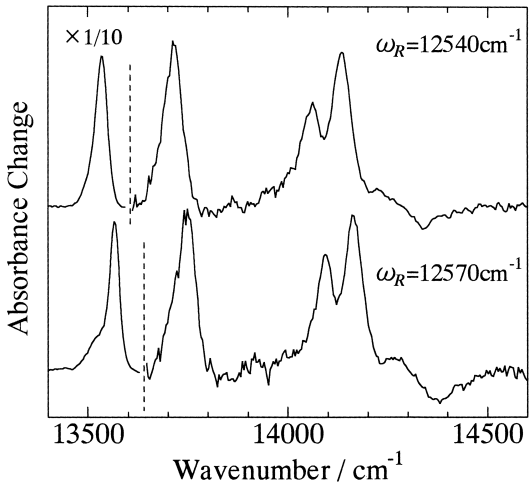

Fig. 3. Absorbance changes induced by the Raman pump pulses with wavenumbers of 12540 and 12570 cm^{-1}. The time difference of the Raman pump pulse is $\Delta t = 0.0$ ps. The probe delay after the 397 nm pump pulse is $t_d = 0.7$ ps.

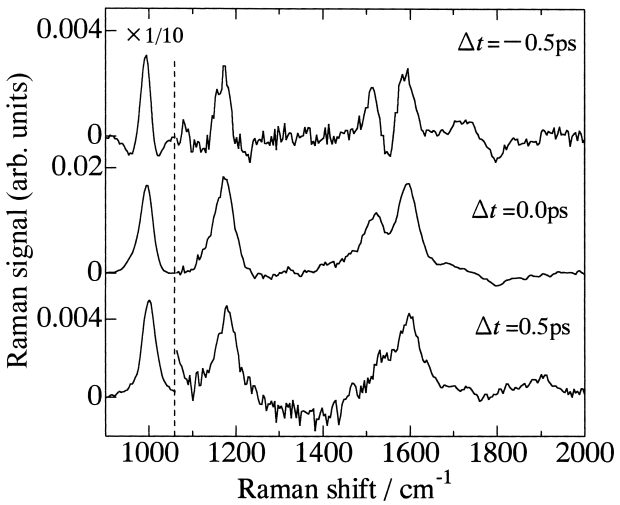

Fig. 4. Raman signals on anti-Stokes side induced by the Raman pump pulses with the time difference of $\Delta t = -0.5$, 0.0, and 0.5 ps. The probe delay after the 397 nm pump pulse is $t_d = 0.7$ ps.

Therefore, the observed signals are assigned to the stimulated Raman scattering also from the temporal dependence on the Raman pump pulse.

Time-Resolved Raman Signals. Figure 5 shows the time-resolved Raman signals on the anti-Stokes side in β-carotene after the 397 nm pump. Since the intensity of the Raman pump pulse decreases due to the absorption of the transient states, the Raman signal at each delay time is normalized using a Raman line of benzene observed at 990 cm^{-1}. The hatched signal at 1590 cm^{-1} is due to benzene. However, the 1170 cm^{-1} signal is partly due to β-carotene, because the observed signal is larger than the hatched signal derived from the intensities of other lines of benzene. The 1520 and 1170 cm^{-1} lines of β-carotene are respectively assigned to the totally symmet-

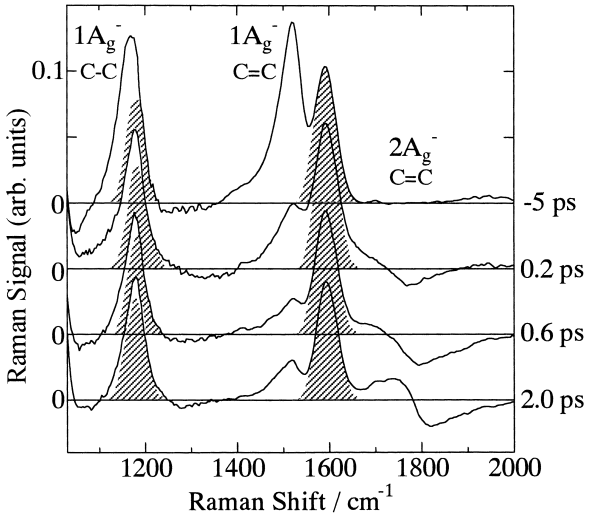

Fig. 5. Time-resolved Raman signals on anti-Stokes side at several delay times after the 397 nm pump pulse in all-*trans*-β-carotene. Hatched signals are due to the solvent.

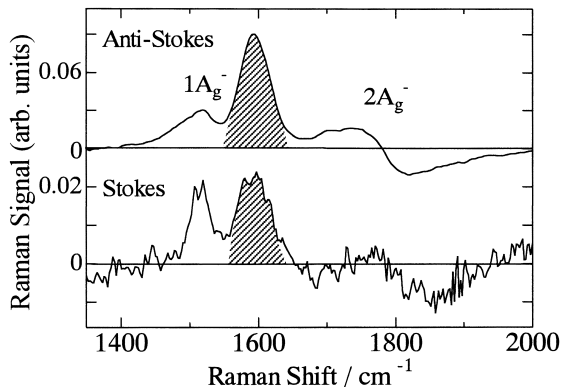

Fig. 6. Time-resolved Raman signals on anti-Stokes side and Stokes side. The delay time after the 397 nm pump pulse is t_d = 2.0 ps. The Raman loss signal on the anti-Stoke side and the Raman gain signal on the Stokes side are plotted as positive. Hatched signals are due to the solvent.

ric C=C stretching vibration (the ν_1 mode) and the in-phase C–C stretching vibration (the ν_2 mode) of the $1A_g^-$ ground state. They decrease after the 397 nm photoexcitation because of the depletion of the ground state. The Raman signal due to the transient state has already been observed around 1790 cm^{-1} by picosecond Raman studies and assigned to the ν_1 mode of the $2A_g^-$ excited state.[12,18,19] In this study, the transient Raman signal is also observed around 1790 cm^{-1}, but the spectral and temporal features are remarkably interesting. The signal at 0.2 ps has a negative peak at 1770 cm^{-1}, but it becomes broad and shifts to 1790 cm^{-1} at 0.6 ps. At 2.0 ps, the signal has a dispersive shape. At the longer delay times, the dispersive signal intensity decreases without changing the spectral shape.

Equation 7 predicts that an inverse or dispersive Raman signal will appear on the anti-Stokes side in cases of near resonance, but the signal on the Stokes side cannot have an inverse and dispersive shape as shown in Eq. 6. Figure 6 shows the

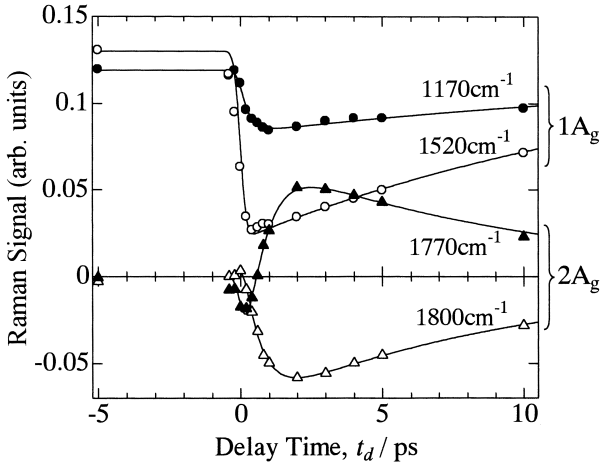

Fig. 7. Temporal profiles of Raman signals. Open and filled circles represent the signals due to the $1A_g^-$ ground state. Open and filled triangles represent the signals due to the $2A_g^-$ excited state. Solid lines are the best fits to the data assuming exponential rise and decay components.

Raman signals on the anti-Stokes and Stokes sides at the delay time of 2.0 ps. The dispersive shape is observed on both sides. Such a result cannot be explained by the near resonance. Moreover, the 12570 cm^{-1} Raman pump pulse is far resonance from the transient absorption due to the $2A_g^-$ state which has the peak at 17500 cm^{-1} and the width of about 600 cm^{-1}. Therefore, each Raman signal observed in this study should have a Lorentzian shape.

The inverse and dispersive shapes can be interpreted if one considers vibrational excited levels. Since the vibrational relaxation takes place in sub-picosecond and picosecond regions, it should be considered in the femtosecond study. When the vibrational levels a and c in Fig. 1(a) have the populations of $N_a(t_d)$ and $N_c(t_d)$, respectively, the nonlinear susceptibility can be written as

$$\chi^{(3)}_{\mathrm{Raman}}(\omega,t_d) \propto \pm \frac{N_a(t_d)-N_c(t_d)}{\omega-\omega_R \pm \omega_{ca}+i(\gamma_v+\gamma_R)} \qquad (9)$$

where plus and minus signs correspond to the signals on the Stokes and anti-Stokes sides, respectively. If N_c is larger than N_a, the Raman signals have inverse signs to the normal Raman gain and Raman loss signals.

The signal observed around 1790 cm^{-1} changes the center frequency and becomes dispersive. It can be simulated using two Lorentzian curves centered at 1770 and 1800 cm^{-1}. The temporal dependence of the simulated Raman signals are plotted in Fig. 7. Both the 1770 and 1800 cm^{-1} signals are assigned to the $2A_g^-$ state from the temporal dependence. The 1770 cm^{-1} signal appears as negative with a time constant of 0.35 ps. Then it becomes positive with a time constant of 0.6 ps. Finally it decreases with the lifetime of the $2A_g^-$ state 8.8 ps. The 1800 cm^{-1} signal is always negative. It appears with the time constant of 0.6 ps and decreases with the 8.8 ps lifetime. The negative Raman signal means the Raman transition from an upper vibrational level to a lower vibrational level.

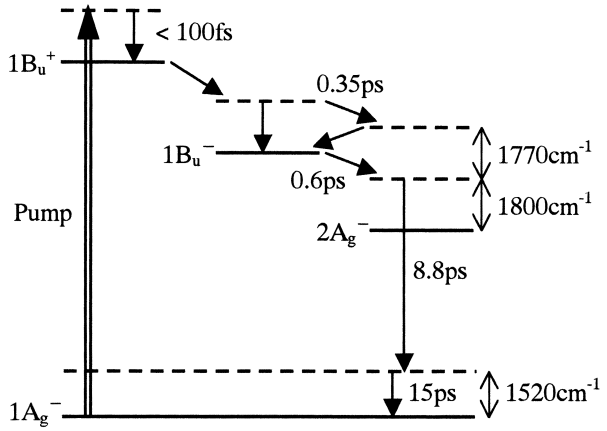

Fig. 8. Schematic energy diagram of all-*trans*-β-carotene and relaxation kinetics after photoexcitation. Dashed lines represent vibrational excited levels of each state.

Therefore, the negative 1800 cm^{-1} signal is assigned to the transition from the $j = 1$ vibrational level to the $j = 0$ level of the ν_1 mode in the $2A_g^-$ state (the 0–1 Raman transition). According to this assignment, the 1770 cm^{-1} line is assigned to the transition between the $j = 2$ and $j = 1$ levels in the $2A_g^-$ state (the 1–2 Raman transition). The kinetics can be explained by vibrational relaxation of the $2A_g^-$ state. The initial negative signal at 1770 cm^{-1} is due to the larger population in the $j = 2$ level. Then the vibrational relaxation to the $j = 1$ level takes place with the time constant of 0.6 ps. Therefore, the 1770 cm^{-1} signal becomes positive and the negative 1800 cm^{-1} signal appears. The Raman signals around 1790 cm^{-1} have not changed the spectral feature at the delay times longer than 2.0 ps. This means that the vibrational relaxation from the $j = 1$ level to the $j = 0$ level is slower than the internal conversion to the ground state.

The 1520 and 1170 cm^{-1} Raman signals due to the $1A_g^-$ ground state decrease instantaneously after the 397 nm pump as shown in Fig. 7. The recovery of the Raman signal has a time constant of 15 ps. It is longer than the lifetime of the $2A_g^-$ state. The slow recovery is explained by the vibrational relaxation of the ground state. The internal conversion from the $2A_g^-$ state generates hot vibrational levels of the ground state and the slow vibrational relaxation with the time constant of 15 ps occurs in the ground state.

Relaxation Kinetics of All-*trans*-β-Carotene. The relaxation kinetics in β-carotene can be interpreted using the energy diagram shown in Fig. 8. First, the vibrational excited level of the $1B_u^+$ state is photoexcited by the 397 nm pump pulse. Since the vibrational relaxation of the $1B_u^+$ state is very fast,[6,10] the initial photogenerated state observed in this study is the lowest vibrational level of the $1B_u^+$ state. Then, the $1B_u^+$ state converts to the $2A_g^-$ state through the $1B_u^-$ state with the time constant of 0.35 ps. Since the highly vibrational excited level ($j = 2$) of the $2A_g^-$ state is generated at this time, the negative Raman signal is observed at 1770 cm^{-1}. The vibrational relaxation from the $j = 2$ level to the $j = 1$ level occurs with the time constant of 0.6 ps. Therefore, the 1770 cm^{-1} signal becomes positive and the negative signal appears at 1800 cm^{-1}. Finally, the internal conversion to the $1A_g^-$ ground state takes place from the $j = 1$ level of the $2A_g^-$ state with the lifetime of 8.8 ps, because the vibrational relaxation from the $j = 1$ level to the $j = 0$ level is slower than the internal conversion. The vibrational relaxation in the ground state is observed as the slow recovery of the Raman signal with the time constant of 15 ps.

The difference of the Raman shifts between the 1–2 and 0–1 transitions can be explained by the vibrational coupling. The vibrational excited levels of the $2A_g^-$ and $1A_g^-$ states in carotenoids are strongly coupled through the ν_1 mode.[18,19] The coupling pushes down the $j = 1$ level of the $1A_g^-$ ground state and pushes up the $j = 1$ level of the $2A_g^-$ state. The $j = 2$ levels are also affected by the coupling, but the shift is expected to be smaller because of the smaller coupling between higher vibrational levels. Therefore, the 1–2 transition of the $2A_g^-$ state has narrower energy gap than the 0–1 transition.

The fast and slow vibrational relaxation of the $2A_g^-$ state can be explained in terms of the $1B_u^-$ state. Since the $1B_u^-$ state in the crystalline β-carotene has been found at 1880 cm^{-1} above the $2A_g^-$ state,[4] it is expected to exist between the $j = 1$ and $j = 2$ levels of the $2A_g^-$ state. The ultrafast vibrational relaxation until the $j = 1$ level is considered to be assisted by the $1B_u^-$ state. A small spectral change due to the fast vibrational relaxation is observed as the 1.0 ps rise component in the absorbance change at 17500 cm^{-1}. A similar spectral change observed in lycopene[9] can be explained also by the fast and slow vibrational relaxation of the $2A_g^-$ state, because lycopene has similar energy levels to those of β-carotene.[4] However, the photoinduced absorbance change in the long carotenoids has a very large spectral change.[7] The large change suggests the vibrational relaxation to the $j = 0$ level of the $2A_g^-$ state. The difference from β-carotene and lycopene appears as smaller separations of the energy levels in longer carotenoids. The $1B_u^-$ state in longer carotenoids is expected to become lower than the $j = 1$ level of the $2A_g^-$ state and to assist the vibrational relaxation to the $j = 0$ level. The systematic investigation of carotenoids with different polyene lengths may clarify the mechanisms of the fast and slow vibrational relaxation in the $2A_g^-$ excited state.

Conclusion

The ultrafast dynamics of the time-resolved Raman signal in all-*trans*-β-carotene has been investigated. The observed signals have been analyzed considering the resonance effect to highly excited states. The stimulated Raman signals are distinguished from the other resonant signals using the spectral feature and the dependence on the Raman pump pulse. A model of the relaxation kinetics in β-carotene has been proposed considering the vibrational relaxation of the excited states. The negative Raman signal indicates that the vibrational excited levels of the $2A_g^-$ state are generated after the photoexcitation. The vibrational relaxation of the $2A_g^-$ state is very fast until the $j = 1$ vibrational level, but that from the $j = 1$ level to the $j = 0$ level is slower than the internal conversion to the ground state. The fast and slow vibrational relaxations are interpreted in terms of the assistance of the $1B_u^-$ state which exists between the $j = 2$ and $j = 1$ levels. Since the energy level is very sensitive to energy transfer rates to other molecules, the vibrational relaxation of the excited states in carotenoids should be

considered when studying the relaxation kinetics and energy transfer in photosynthesis.

This research was supported in part by a grant from the Sumitomo Foundation.

References

1 Y. Koyama, M. Kuki, P. O. Andersson, and T. Gillbro, *Photochem. Photobiol.*, **63**, 243 (1996).
2 H. A. Frank and R. J. Cogdell, *Photochem. Photobiol.*, **63**, 257 (1996).
3 P. Tavan and K. shulten, *Phys. Rev. B*, **36**, 4337 (1987).
4 T. Sahima, Y. Koyama, T. Yamada, and H. Hashimoto, *J. Phys. Chem. B*, **104**, 5011 (2000).
5 A. P. Shreve, J. K. Trautman, T. G. Owens, and A. C. Albrecht, *Chem. Phys. Lett.*, **178**, 89 (1991).
6 H. Kandori, H. Sasabe, and M. Mimuro, *J. Am. Chem. Soc.*, **116**, 2671 (1994).
7 P. O. Andersson and T. Gillbro, *J. Chem. Phys.*, **103**, 2509 (1995).
8 M. Ricci, S. P. Bradforth, R. Jimenez, and G. R. Fleming, *Chem. Phys. Lett.*, **259**, 381 (1996).
9 J.-P. Zhang, C.-H. Chen, Y. Koyama, and H. Nagae, *J. Phys. Chem. B*, **102**, 1632 (1998).
10 S. Akimoto, I. Yamazaki, S. Takeuchi, and M. Mimuro, *Chem. Phys. Lett.*, **313**, 63 (1999).
11 J.-P. Zhang, R. Fujii, P. Qian, T. Inaba, T. Mizoguchi, Y. Koyama, K. Onaka, Y. Watanaba, and H. Nagae, *J. Phys. Chem. B*, **104**, 3683 (2000).
12 H. Nagae, M. Kuki, J.-P. Zhang, T. Sashima, Y. Kumai, and Y. Koyama, *J. Phys. Chem. A*, **104**, 4155 (2000).
13 G. Cerullo, G. Lanzani, M. Zavelani-Rossi, and S. De Silvestri, *Phys. Rev. B*, **63**, 241104 (2001).
14 M. Yoshizawa, H. Aoki, and H. Hashimoto, *Phys. Rev. B*, **63**, 180301 (2001).
15 M. Yoshizawa, H. Aoki, and H. Hashimoto, *Carotenoid Science*, **4**, 15 (2001).
16 T. Elsaesser and W. Kaiser, *Annu. Rev. Phys. Chem.*, **42**, 83 (1991).
17 A. Damjanovic, T. Ritz, and K. Schulten, *Phy. Rev. E*, **59**, 3293 (1999).
18 H. Hashimoto and Y. Koyama, *Chem. Phys. Lett.*, **163**, 251 (1989).
19 T. Noguchi, S. Kolaczkowski, C. Arbour, S. Aramaki, G. H. Atkinson, H. Hayashi, and M. Tasumi, *Photochem. Photobiol.*, **50**, 603 (1989).
20 M. Delhaye, "Lasers in Physical Chemistry and Biophysics,"Elesevier, Amsterdam (1975), p. 213.
21 J. Ternerm, T. G. Spiro, M. Nagumo, M. F. Nicol, and M. A. El-Sayed, *J. Am. Chem. Soc.*, **102**, 3238 (1980).
22 M. Coopey, H. P. Valat, and B. Alpert, *Nature*, **284**, 568 (1980).
23 P. J. Reid, S. J. Doig, and R. A. Mathies, *Chem. Phys. Lett.*, **156**, 163 (1989).
24 T. L. Brack and G. H. Atkinson, *J. Phys. Chem.*, **95**, 2351 (1991).
25 K. Iwata, S. Yamaguchi, and H. Hamaguchi, *Rev. Sci. Instrum.*, **64**, 2140 (1993).
26 J. W. Petrich and J. L. Martin, *Chem. Phys.*, **131**, 31 (1989).
27 M. Yoshizawa, Y. Hattori, and T. Kobayashi, *Phys. Rev. B*, **49**, 13259 (1994).
28 K. Tanaka, H. Ohtake, and T. Suemoto, *J. Lumin.*, **60 & 61**, 716 (1994).
29 Y. Huang and J. B. Hopkins, *J. Phys. Chem.*, **100**, 9585 (1996).
30 M. Yoshizawa and M. Kurosawa, *Phys. Rev. A*, **61**, 013808 (2000).
31 S. Saikan, N. Hashimoto, T. Kushida, and K. Namba, *J. Chem. Phys.*, **82**, 5409 (1985).